Research, Society and Development, v. 9, n. 9, e486997499, 2020
(CC BY 4.0) | ISSN 2525-3409 | DOI: http://dx.doi.org/10.33448/rsd-v9i9.7499

Sistema de projeção de interferogramas simples e de baixo custo para a perfilometria de pequenas peças automotivas: comparação com um dispositivo comercial

Simple and low-cost interferogram projection system for small-size automotive parts profilometry: benchmarking with a commercial apparatus

Sistema de proyección simple e de bajo costo para la medición perfilometrica de pequeñas piezas automotrizes: comparación con un dispositivo comercial

Received: 12/08/2020 | Reviewed: 20/08/2020 | Accept: 23/08/2020 | Published: 27/08/2020

Marlene Correa Henrique
ORCID: https://orcid.org/0000-0002-5321-7655
Unidade de Pós-Graduação, Extensão e Pesquisa, CEETEPS, Brazil
E-mail: marlene.c.henrique@gmail.com
Marcelo Tadao Saita
ORCID: https://orcid.org/0000-0002-9612-0992
Instituto de Pesquisas Tecnológicas, Brazil
E-mail: marcelo.saita@hotmail.com
Luiz Felipe Gonçalves Dib
ORCID: https://orcid.org/0000-0001-6787-5408
Faculdade de Tecnologia de São Paulo, Brasil
E-mail: lfgdib@fatecp.br
Eduardo Acedo Barbosa
ORCID: https://orcid.org/0000-0003-1107-9933
Unidade de Pós-Graduação, Extensão e Pesquisa, CEETEPS, Brazil
E-mail: ebarbosa@fatecsp.br
Edney Eboli dos Santos
ORCID: https://orcid.org/0000-0001-7423-5070
Unidade de Pós-Graduação, Extensão e Pesquisa, CEETEPS, Brazil
E-mail: eebolis@gmail.com
Antonio César Galhardi
ORCID: https://orcid.org/0000-0002-8838-6870
Unidade de Pós-Graduação, Extensão e Pesquisa, CEETEPS, Brazil
E-mail: eebolis@gmail.com

Resumo

A medição de relevo tridimensional (3D) tornou-se muito importante na indústria e em muitos outros sistemas produtivos. Técnica ópticas propiciam muitas características atraentes para este tipo de medida devido à sua precisão, confiabilidade, exatidão e capacidade de medir objetos pequenos e frágeis. Neste trabalho, relatamos o estudo, o desenvolvimento e o desempenho de um dispositivo óptico de baixo custo baseado na projeção de interferogramas para a medição do relevo submilimétrico de placas poliméricas que contêm texturas biomiméticas usadas na indústria automotiva. O interferograma foi gerado por um interferômetro de Twyman-Green iluminado por um laser verde emitindo em 532 nm. A medição foi feita por técnicas de deslocamento de fase (*phase shifting*) e deconvolução de fase (*phase-unwrapping*) e os resultados foram confrontados com os obtidos por um dispositivo comercial.

Palavras chave: Medição óptica tridimensional; Projeção de interferogramas; Análise de franjas; Interferômetros.

Abstract

Three-dimensional (3D) contouring has become very important in industry and in many other production systems. The optical techniques provide many attractive properties for such measurement due to their precision, reliability, accuracy and ability to measure small and fragile objects. In this work we report the study, the development and the performance of a low-cost optical device based on interferogram projection in order to measure the sub-millimetric relief of polymeric plates containing biomimetic textures used in the automotive industry. The interferogram was generated by a Twyman-Green interferometer illuminated by a 532-nm green laser. The measurement was performed by means of phase-shifting and phase-unwrapping procedures and the results were benchmarked with the ones obtained by a commercial device.

Keywords: Optical 3D measurement; Interferogram projection; Fringe evaluation; Interferometers.

Resumen

La medición de relieve tridimensional (3D) se há vuelto muy importante em la industria y en muchos otros sistemas de producción. Las técnicas ópticas presentan muchas caracteristicas atractivas para este tipo de medición debido a su precisión, confiabilidad, exactitud y

capacidad para medir objetos pequeños y frágiles. Em este trabajo se reporta el estudio, desarollo y desempeño de un dispositivo óptico de bajo costo basado en la proyección de interferogramas para la medición del relieve submilimétrico de placas poliméricas que contienen texturas biomiméticas utilizadas en la industria automotriz. El interferograma se generó mediante un interferómetro Twyman-Green iluminado por un láser verde que emite a 532 nm. La medición se realizó mediante técnicas de desplazamiento de fase (*phase shifting*) y deconvolución de fase (*phase-unwrapping*) y los resultados fuerón comparados com los obtenidos por un dispositivo comercial.

Palabras clave: Medición óptica tridimensional; Projeción de interferogramas; Análisis de franjas; Interferómetros.

1. Introduction

Optical methods for 3D shape measurement have gained increasing relevance and have been applied in several areas of science and technology. Due to their precision and sensitivity, those techniques find applications in electrical engineering (He et al, 2006) and precision mechanics (Son et al, 2002). Since those techniques provide non-contact testing, they are very suitable for measuring delicate and soft textures, like e.g. in quality control of vegetable shape and aging in agricultural engineering (Cardoso et al, 2014) or in evaluation of the retina in ophthalmology procedures (Drexler *et al*, 2001). Low-coherence speckle metrology enabled also good results in lens characterization (Barbosa *et al*, 2013) and laser scanning provided applications in historical restoration (Liang *et al*, 2016). Techniques based on moiré effect, like dual-phase shifting moiré (Chen et al, 2011), projection moiré (Suzuki et al, 1988), and shadow moiré (Du *et al*, 2018) found many applications for surface contouring.

Among the optical techniques, the structured light projection became possibly the one with most commercial relevance with a very large amount of industrial and technological applications, due to its simplicity, reliability and precision. Structured light consists of a geometrically known and spatially periodic light pattern. When this pattern is projected onto a surface with oblique incidence and observed by a proper angle, the resulting light undergoes deformations according to the surface shape (Angelo *et al*, 2019; Jeng, 2011). By evaluating the deformed light pattern one obtains the contour map of the studied surface.

Structured light has been studied for a myriad of applications in biology and medicine (Laughner *et al*, 2012; Van de Giessen *et al*, 2015; McClatchy *et al*, 2017), microscopy (Quan

et al, 2002; He *et al*, 2006), facial recognition (Zhou *et al*, 2009) and roughness and corrosion studies (Windecker *et al*, 1999).

The most common and well-established geometry of structured light is formed by parallel and straight bars or stripes. This geometry can be usually achieved by means of light interference. In this work we propose the use of a Twyman-Green (TG) interferometer illuminated by a solid state laser to generate and to project an interference pattern – the interferogram – formed by straight and parallel fringes to perform the 3D reconstruction of biomimetic micro-textures (patterns inspired in Nature models) for polymeric automotive parts.

In order to evaluate the projected fringe pattern was sequentially phase-shifted with 4 steps of one quarter of a fringe ($\pi/2$ rad) and stored, the so-called four stepping procedure. The four acquired frames are then combined to get the phase map of the studied object. This resulting wrapped phase map is then deconvoluted by means of phase-unwrapping procedures to provide the reconstructed surface. In our work we performed the measurement of biomimetic inspired polymeric structures used in panels for the automotive industry. Those structures were manufactured whether by etching (chemical process) or by laser ablation. We compare the obtained contour maps with the ones obtained with a commercial device.

2. Materials and Methods

In this section the theoretical basis of fringe projection profilometry is briefly discussed and the experimental setup is described.

Our methodological approach consisted firstly of a bibliographic research for a further theoretical and conceptual analysis of the principles and phenomena that support our experimental work. Hence, we opted for a quantitative laboratorial approach (Pereira et al, 2018).

From the theoretical study of light wavefronts, interference and triangulation we built an interferometer to generate the fringe pattern and developed an optical setup in order to achieve the best measurement sensitivity. This optical setup was adjusted in order to confirm by means of the experiments our theoretical prediction. The experiments and all measurements were performed at the Laboratório de Óptica Aplicada at Faculdade de Tecnologia de São Paulo (Fatec-SP).

2.1 Theory of shape measurement by interference fringe projection

Figure 1 shows the oblique incidence of a uniform interferogram (a regularly spaced fringe pattern) onto the studied surface on *xy*-plane. Consider that a CCD collects the image of the surface covered by the resulting contour fringes along the *z*-axis (the "observer" in Figure 1).

If the illuminated surface is planar, the contour pattern is formed by straight and parallel stripes which comprise the interferogram. Otherwise, if the surface is not perfectly flat, the projected interferogram will appear deformed to the observed according to the surface relief.

Figure 1. Light incidence onto the studied surface.

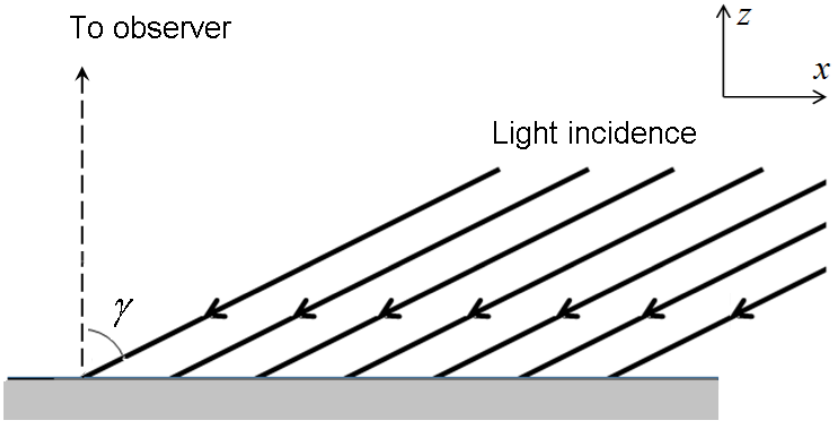

Source: The authors.

After acquiring four phase-shifted interferograms with intensities I_0, I_1, I_2 and I_3 the phase map $\Phi(x, y)$ containing the coded surface contour is determined according to Kreath (1988):

$$\Phi(x,y) = \arctan\left[\frac{I_3(x,y) - I_1(x,y)}{I_0(x,y) - I_2(x,y)}\right], \quad (1)$$

where (*x*,*y*) is a point of the illuminated surface. By performing the phase unwrapping procedure (Ghiglia et al, 1987) the phase is deconvoluted. In 8-bit imaging systems like the

one used in this work the phase is displayed in 256 gray levels, ranging from 0 (black, lowest *z*-level) to 255 (white, highest *z*-level).

The phase map appears pseudo-tilted by an angle θ relatively to the z-axis of Figure 1. If a point P with coordinates ($x_p^{'}, y_p^{'}$) has a pseudo height coordinate $z_p^{'}$, the correct height coordinate z_p is obtained by the operation bellow:

$$x_p = x_p^{'} \tag{2a}$$

$$z_p = -\sin\theta\, x_p^{'} + \cos\theta\, z_p^{'} \tag{2b}$$

By applying the coordinate transformation of equation (2) the reconstructed surface is positioned in the correct position with respect to the observer.

2.2 Experimental setup

The optical arrangement is shown in Figure 2. A laser beam originated from a frequency-doubled Nd:YAG laser with emission centered at λ = 532 nm is filtered by the spatial filter and beam expander SF to illuminate the Twyman-Green interferometer TG The light emerging from the TG hits the object surface at an incidence angle $\gamma = 70^{o}$ after being reflected by folding mirror M.

Figure 2. Optical setup: SF, spatial filter; TG, Twyman-Green interferometer; PZT-M, mirror attached to a piezo transducer; M, mirror; CCD, camera.

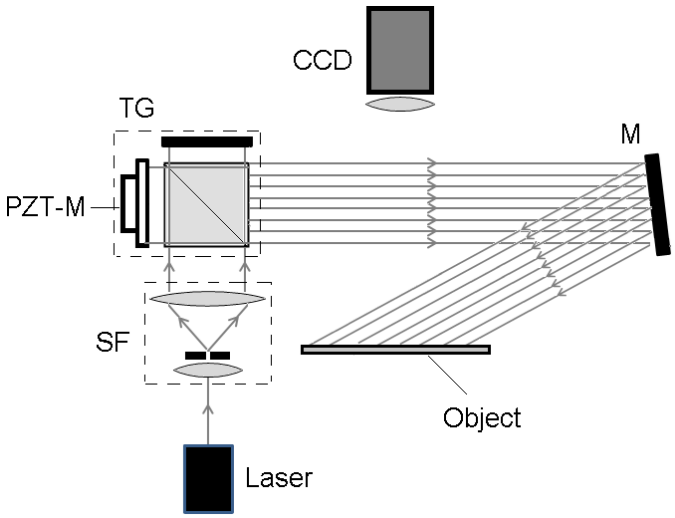

Source: The authors.

The imaging system shown in Figure 2 is comprised by a 640-lines monochrome CCD camera (pixel size 15 μm) and a computer for image acquiring and further processing. One of the mirrors of the interferometer (PZT-M in Figure 2) was attached and supported by a piezoelectric transducer in order to phase shift the interferograms in the phase stepping procedures.

For the sake of comparison, the patterns were also scanned by a high-resolution commercial device, the optical contact profilometer model 3D UHD Scanner from the AKK® company. The resolution of this system is 3600-dpi with a scanning area of 20 x 20 mm^2.

3. Results and Discussion

We measured biomimetic patterns produced by etching or by laser ablation inspired in corn grains and in seaweeds. The results below show the 3D reconstructions of the patterns obtained by fringe projection, four-stepping phase mapping and phase unwrapping performed by the branch-cut method. After each measurement, we obtained the height profile of the pattern and compared it with the correspondent measurement performed by the 3D UHD Scanner.

3.1 Corn grains

One of the four phase-shifted frames of the 6.0 x 4.5-mm^2 ($x \times y$) surface area of the corn grain pattern made by laser ablation is shown Figure 3a. Notice that the surface is covered by the interference fringes which became deformed due to the surface relief. Figure 3b shows the phase map after combining the four frames in equation (1). The unwrapped phase of the sample from the phase map is shown in Figure 3c.

This figure mistakenly suggests that the object plane is tilted with respect to the z-axis of Figure 1, with the left side (dark) of the frame having lower z-values and the right side (bright) of the frame having higher z-values.

In order to compensate this pseudo-inclination, equations (2a) and (2b) were applied to provide the 3D reconstructed surface shown in Figure 3d, with z given in arbitrary units (a.u.).

Figure 3. Analysis of the corn grain pattern made by laser: a – fringe projection; b – phase map; c - unwrapped phase; d - 3D reconstruction.

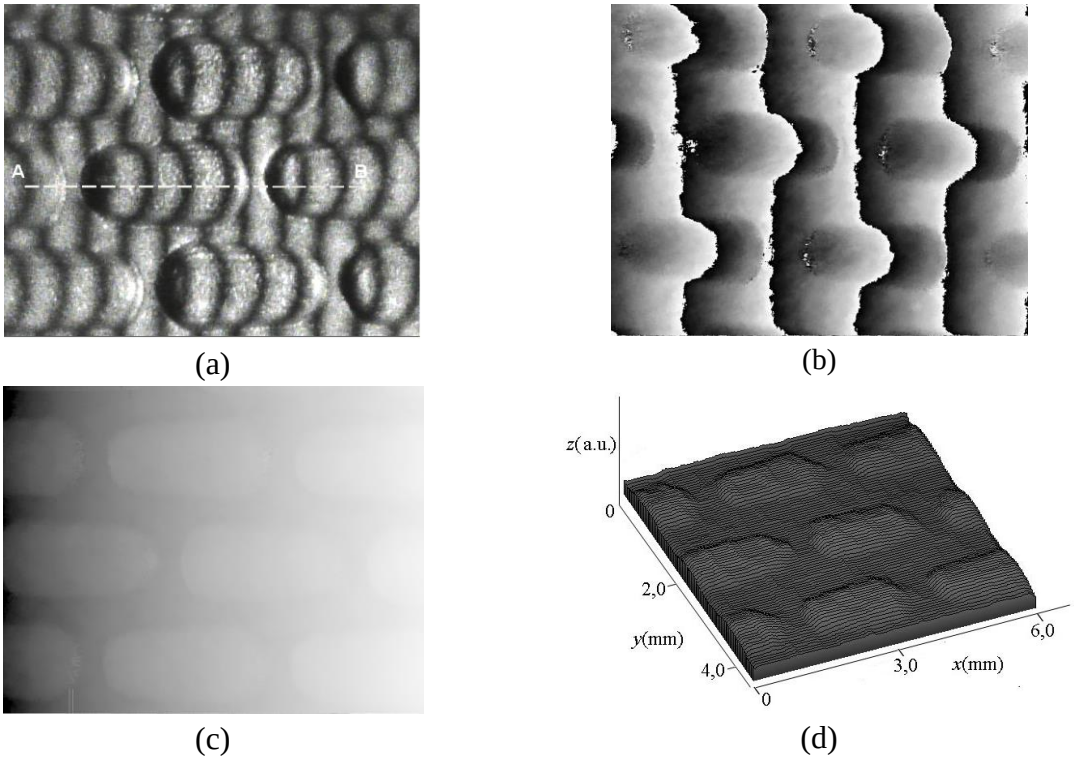

(a) (b) (c) (d)

Source: The authors.

Figure 4a shows the profile of the corn grain pattern measured by our method, while Figure 4b shows the same corresponding profile obtained by the commercial 3D UHD scanner. Both curves were obtained along line AB shown in Figure 3A. At first glance a good similarity between both measurements can be observed, but there are also some discrepancies, however. In the central "corn grain", the distance between the superior edges (points P and Q in both graphs) is ~ 1,7 mm in the fringe projection measurement, while it is ~2,1 mm obtained by the 3D UHD device. It is due to the fact that the sides of the "grains" have different inclinations in each measurement, which in turn can be mainly attributed to a higher resolution of the commercial device, if compared to our home-made, fringe projection profilometer. The "grain" heights obtained by both measurement are different also, ~140 μm for the fringe projection system and ~166 μm for the 3D UHD scanner.

Figure 4. Comparison of the profiles of the laser machined corn grains sample measured by a – fringe projection and b – 3D UHD commercial apparatus.

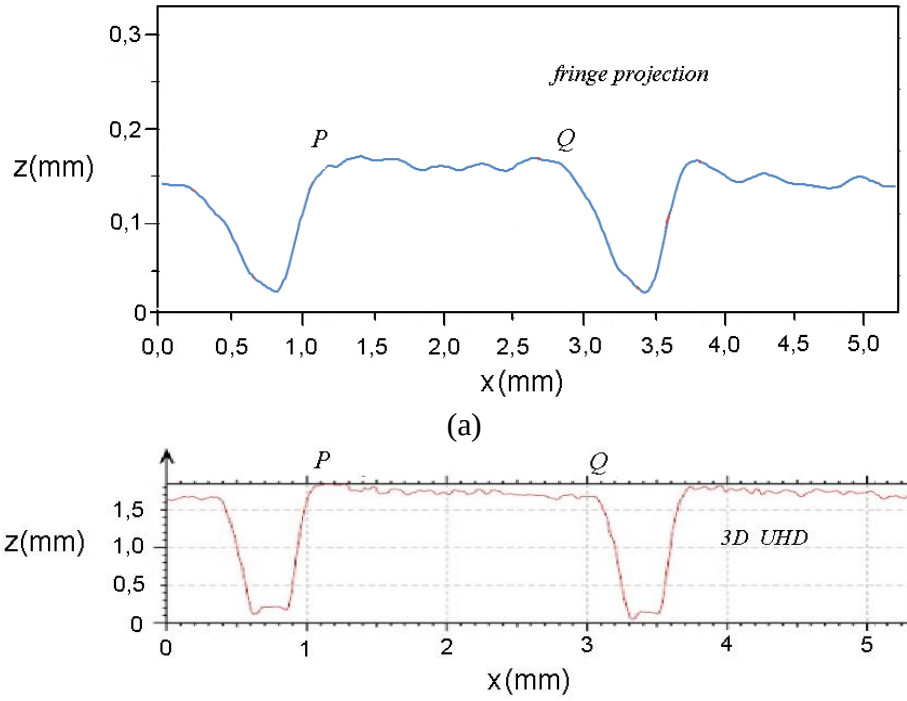

(a)

(b)

Source: The authors.

3.2 Seaweed

Figure 5 shows analogous results obtained for the biomimetic seaweed polymeric sample after applying the same procedures described in section 2 and applied in section 3.1. The etched seaweed pattern illuminated by the interference fringes is shown in Figure 5a while Figure 5b shows the resulting 3D reconstruction.

Figure 5. Analysis of the seaweed pattern made by etching: a – illuminated pattern by uniform interferogram; b - 3D reconstruction.

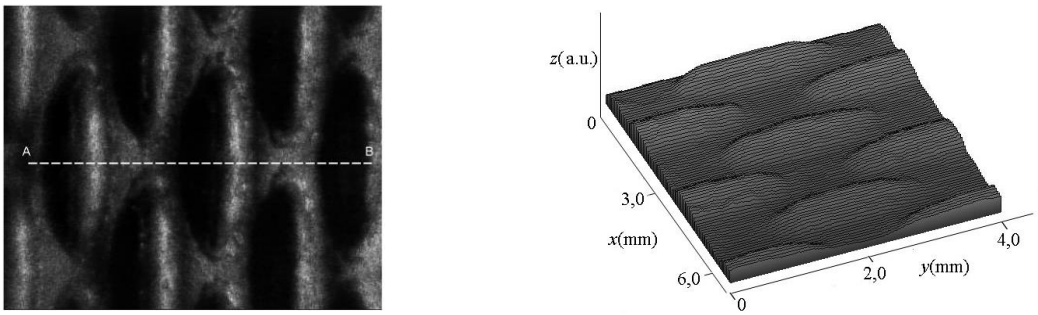

(a) (b)

Source: The authors.

Figure 6 compares the profiles of the height coordinate *z* of the seaweed patterns along lines AB shown in Figure 5a. One observes that the lower resolution of our system was not able to reproduce the correct inclination of the sides of the individual seaweeds, quite much similar to what was observed in the previous measurement. For this reason, the width of half-maximum – distance between points P and Q in Figures 6a and 6b – is approximately 10 % higher in the fringe projection measurement, Figure 6a. Nevertheless, one notes also a very good similarity of the height coordinates *z* for both measurements, with discrepancies not exceeding 5 %.

Figure 6. Comparison of height profiles of the etched seaweed sample measured by a – fringe projection and b – 3D UHD commercial apparatus.

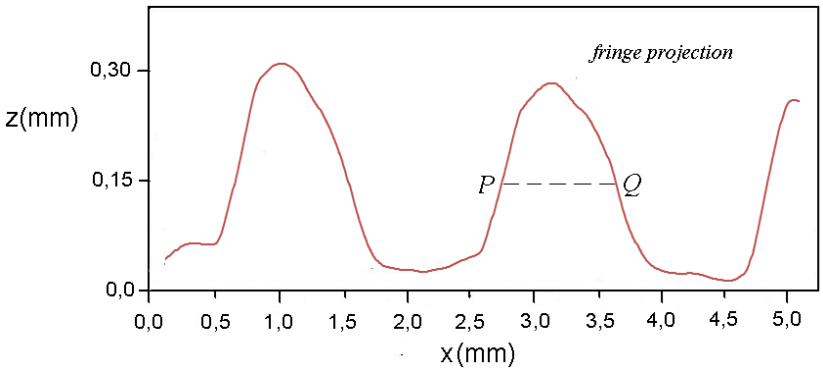

(a)

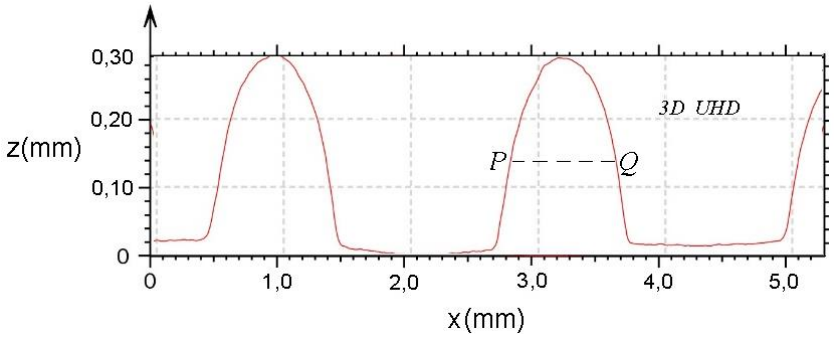

(b)

Source: The authors.

Another noticeable difference between the graphs 6a and 6b is the symmetry of the elevations. While the benchmark measurement of Figure 6b has symmetric elevations with respect to the z-axis, the fringe projection elevations shown in Figure 6a are remarkably asymmetric. This difference may be mainly attributed to the fact the sample was illuminated from one side only, as shown in Figure 1.

A possible solution for this error is using two illuminating light patterns, each one coming from the opposite sides with respect to the z-axis. Hence, two 3D reconstructions could be obtained and averaged in order to provide the resulting object contouring.

4. Conclusion

A simple and reliable optical device for surface contouring was developed and its effectiveness was demonstrated. The simple, low-cost and easily available components of the optical setup allowed for the construction of a cost-effective equipment which points out for applications in industrial plants and other production systems.

Biomimetic polymeric samples with details and structures of the order of 150 μm were successfully reconstructed and resolved. Our device was benchmarked with a high-resolution commercial apparatus and the results showed compatible performances concerning the shape and the dimensions of the structures.

Some improvements and further development must be implemented, nevertheless. Fringe evaluation by Fourier transform would be very suitable for such measurement and could provide faster testing without the need of a transducer and a moveable mirror to perform phase stepping.

As discussed in the previous section, the use of two illuminating light patterns could enhance the measurement accuracy and without turning the process to be significantly more

complex. The use of higher resolution - and widely available - cameras would undoubtedly allow for more precise results either without significantly rising the cost of the device.

References

Angelo, J. P., Chen, S.-J., Ochoa, M., Sunar, U., Gioux, S. & Intes, X., (2019). Review of structured light in diffuse optical imaging, *Journal of Biomedical Optics* 24, 7. 071602. https://doi.org/10.1117/1.JBO.24.7.071602

Barbosa, E. A., Silva, D. M., Nascimento, C. E., Galvão, F. L., & Mittani, J. C. R. (2013). Progressive power lens measurement by low coherence speckle interferometry, *Optics and Lasers in Engineering*, 51 (7) 898-906. https://doi.org/10.1016/j.optlaseng.2013.02.007

Cardoso, K. C., Gazzola, J., & Dal Fabbro, I. M., (2014). Application of *moiré* technique on strain analysis in farm machinery elements. *Revista de Ciências Agronômicas* 45, 3 . https://doi.org/10.1590/S1806-66902014000300007

Chen, L. C., & Tsai, L. H., (2011). Dual Phase-shifting Moiré Projection with Tunable High Contrast Fringes for Three-Dimensional Microscopic Surface Profilometry. *Physics Procedia* 19. 67–75. https://doi.org/10.1016/j.phpro.2011.06.127

Creath, K. (1988), Phase measurement Techniques. *In Progress in Optics*, Elsevier, p. 349-393. https://doi.org/10.1016/S0079-6638(08)70178-1

Drexler, W., Morgner, U., Ghanta, R. K., Kärtner, F. X., Schuman, J. S., & Fujimoto, J. G., (2001). Ultrahigh-resolution ophthalmic optical coherence tomography, *Nature Medicine* 7, 4 502–507. https://doi.org/10.1038/86589

Ghiglia, D. C., Mastin, G. A., & Romero, L. A., (1987). Cellular-automata method for phase unwrapping, *Journal of the Optical Society of America A* 4. 210–219. https://doi.org/10.1364/JOSAA.4.000267

He, X., Sun, W., Zheng, X., & Nie, M., (2006). Static and dynamic deformation measurements of micro beams by the technique of digital image correlation, *Key Engineering Materials* 326-328. 211–214. https://doi.org/10.4028/www.scientific.net/KEM.326-328.211

Jeng, J., (2011) Structured-light 3D surface imaging: a tutorial. *Advances in Optics and Photonics* 3, 128–160. https://doi.org/10.1364/AOP.3.000128

Laughner, J. I., Zhang, S., Li, H., Shao, C. C., & Efimov, I. R., (2012). Mapping cardiac surface mechanics with structured light imaging. *Am J Physiol Heart Circ Physiol* 303, 6 H712-20, https://doi.org/10.1152/ajpheart.00269.2012

Liang, X., Kankare, V., Hyyppä, J., Wang, Y., Kukko, A., Haggrén, H., Yu, X., Kaartinen, H., Jaakkola, A., Guan, F., Holopainen, M., & Vastarant, M., (2016). Terrestrial laser scanning in forest inventories. *ISPRS Journal of Photogrammetry and Remote Sensing 115*. 63-77. https://doi.org/10.1016/j.isprsjprs.2016.01.006

McClatchy, D. M., Hoopes, P. J., Pogue, B. W., & Kanick, S. C. (2017). Monochromatic subdiffusive spatial frequency domain imaging provides in-situ sensitivity to intratumoral morphological heterogeneity in a murine model. *Journal of. Biophotonics* 10, 2. 211–216. https://doi.org/10.1002/JBIO.201600181

Pereira, A. S., Shitsuka, D. M., Parreira, F. J., & Shitsuka, R. (2018). *Metodologia da pesquisa científica*. [*e-book*]. Santa Maria. UAB/NTE/UFSM.

Quan, C., Tay, C. J., He, X. Y., Kang, X., & Shang, H. M., (2002). Microscopic surface contouring by fringe projection method. *Optics and Laser Technology* 34, 7. 547–552. https://doi.org/10.1016/S0030-3992(02)00070-1

Son, S., Park, H., & Lee, K. H., (2002). Automated laser scanning system for reverse engineering and inspection. *International Journal of Machine Tools and Manufacture*, 42, I8 889-897. https://doi.org/10.1016/j.phpro.2011.06.127

Van de Giessen, M., Angelo, J. P., & Gioux, S., (2015). Real-time, profile-corrected single snapshot imaging of optical properties. *Biomedical Optics Express* 6,10. 4051–4062. https://doi.org/10.1364/BOE.6.004051

Windecker, R., Franz S., & Tiziani, H.-J. (1999) Optical roughness measurements with fringe projection, *Applied Optics* 38 (13) 2837-2842. https://doi.org/10.1364/AO.38.002837

Zhou, G., Li, Z., Wang, C., & Shi, Y., (2009) A novel method for human expression rapid reconstruction, *Tsinghua Science & Technology* 14. 62-65. https://doi.org/10.1016/S1007-0214(09)70068-9

Percentage of contribution of each author in the manuscript

Marlene Correa Henrique – 20%

Marcelo Tadao Saita – 20%

Luiz Felipe Gonçalves Dib – 20%

Eduardo Acedo Barbosa – 10%

Edney Eboli dos Santos – 20%

Antonio César Galhardi – 10%